Journal of Materials Chemistry A

Accepted Manuscript

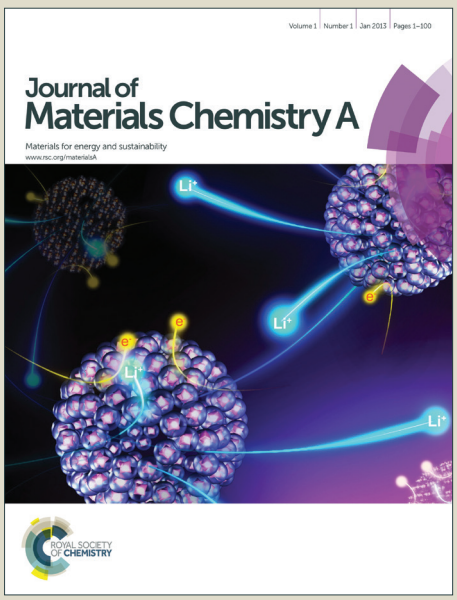

ROYAL SOCIETY OF CHEMISTRY

www.rsc.org/materialsA

TOC graphics

An enhanced conversion efficiency of ~3.1% was achieved for non-colloidal PbS/CdS thin film solar cells with proper band alignments.

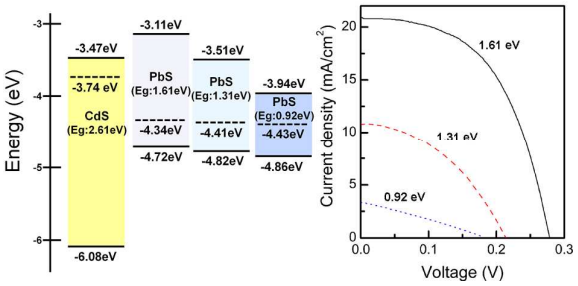

Origin of the enhanced photovoltaic characteristics of PbS thin film solar cells processed at near room temperature

Deuk Ho Yeon‡, Seung Min Lee‡, Yeon Hwa Jo, Jooho Moon and Yong Soo Cho*

Department of Materials Science and Engineering, Yonsei University, Seoul 120-749, Korea

Abstract

An enhanced conversion efficiency of ~3.1 % for PbS/CdS thin film solar cells without the involvement of quantum dots is demonstrated by focusing on the origin of the enhancement. The optical band gap of PbS absorber is optimized toward the higher value by utilizing near room temperature deposition in chemical baths. Only the highest band gap of ~1.61 eV for p-type PbS, which was obtained at 40 ^{o}C, results in a promising band alignment with n-type CdS layer for effective light absorption and charge transfer. Both open circuit voltage and current density increase substantially to 280 mV and 20.93 mA/cm^2, respectively, with the ideal adjustment of the relative band gaps. The variations in crystallite size, surface roughness, the stoichiometry ratio of S/Pb and carrier concentration are discussed as key parameters in relation to the improved band alignment and photovoltaic properties.

Keywords: Lead sulfides, Photovoltaic, Chemical bath deposition, Thin film solar cell

*Corresponding Author:

Tel.: 82-2-2123-5848; fax: 82-2-312-5375.

E-mail address: ycho@yonsei.ac.kr (Yong Soo Cho)

‡These authors contributed equally.

Introduction

Binary metal sulfide-based semiconductors have been widely investigated in an attempt to assess their potential for various optoelectronic and photovoltaic applications due to their unique optical properties.[1-3] Earlier studies have shown that metal sulfides exhibit band gap tunability, which is useful for thin film solar cells.[4,5] There are several techniques to deposit the binary metal sulfide semiconductors, such as chemical bath deposition (CBD), thermal evaporation, spray deposition, and atomic layer deposition process.[6-9] Of those processes, the CBD method has been used for potential solar cell applications because of its simplicity and cost effectiveness in preparing dense thin films at low temperatures.[6]

Among binary metal sulfides, PbS is one of the most extensively investigated materials as a p-type absorber because of its large exciton Bohr radius and high absorption coefficient of ~10^5 cm^{-1} in visible light.[10,11] Many n-type semiconductors, i.e., ZnO, TiO_2, CdS, and Bi_2S_3, have been studied to achieve promising junctions with the p-type PbS for better performance of solar cells.[6,10-12] Among the n-type candidates, CdS is considered as a proper window layer for the PbS absorber due to its high transmittance with a wide band gap of 2.4-2.6 eV and a high carrier concentration of ~10^{18} cm^{-3}.[6,13] The conduction band edge of CdS is much lower compared to those of other n-type sulfide materials, which is capable of offering a higher driving force for carrier transfer from the PbS layer.[13]

While a lot of the recent PbS studies are focusing on the quantum dot (QD) approach, there have been very rare studies dealing with the improvement of photovoltaic characteristics in regular thin films. Hernandez-Borja et al.[14] had reported the chemically-deposited PbS/CdS thin film solar cells with an efficiency of ~1.63 %. Recently, Obaid et al.[6] achieved a similar efficiency of ~1.68 % for the PbS/CdS solar cells prepared by a microwave-assisted chemical bath deposition (CBD) process, which is so far the best performance not concerning the involvement of QDs. However, these studies have limitations in optimizing photovoltaic

properties particularly in terms of crystallite size and thus optical band gap. There has been no report on the band gap alignment at the heterojunction of regular thin films.

In this work, PbS/CdS-based thin film solar cells are fabricated on a fluorine-doped tin oxide (FTO)/glass substrate by a typical CBD process at different temperatures. The aim of present work is to scrutinize the origin of the improved photovoltaic performance in relations to relative band positioning at interfaces between PbS and CdS layers, and to the Pb/S ratio on the film surface. As a consequence, a champion cell efficiency of ~3.10 % is achievable for the PbS thin film possessing the largest band gap of ~1.61 eV when processed at near room temperature.

Experimental Section

CdS/PbS heterojunction solar cells were prepared on FTO-coated soda lime silicate (SLS) glass substrates by chemical bath deposition. First, CdS thin film was grown in a bath of an aqueous solution containing 0.025 M cadmium nitrate ($Cd(NO_3)_2 \cdot 4H_2O$, Kanto chemical, 98%), 0.15 M sodium citrate ($Na_3C_6H_5O_7$, Duksan, 99%), 0.3 M ammonia (NH_4OH, Duksan, 30%) and 0.05 M thiourea (CH_4N_2S, Aldrich, 99%). Ultrasonically-cleaned FTO substrates were vertically immersed into the CdS precursor solution at 80 ^oC for 30 min. The deposition process was repeated twice to obtain a thickness of ~50 nm.

PbS thin films were then grown on the as-deposited CdS film in another aqueous solution containing 0.05 M lead nitrate ($Pb(NO_3)_2$, Kanto chemical, 99.3%), 0.04 M triethanolamine ($C_6H_{15}NO_3$, Aldrich, 98%), 0.2 M sodium hydroxide (NaOH, Duksan, 93%) and 0.06 M thiourea. Different bath temperatures of 40, 60 and 80 ^oC were adopted for the PbS deposition. Deposition time was adjusted to obtain an identical PbS thickness of ~200 nm at each temperature, i.e., 60, 30 and 5 min at 40, 60 and 80 ^oC, respectively. The thickness of PbS films was determined by confirming the minimal level of capacitance in the range of

film thickness from 60 to 320 nm by the capacitance-voltage measurement as suggested elsewhere.[15] After the PbS deposition, the specimens were rinsed with deionized water and dried in N_2 gas. An Al layer with a thickness of ~100 nm was deposited by thermal evaporation.

Surface and cross-sectional microstructures were observed by field emission scanning electron microscopy (FESEM: JSM-7001F, JEOL) equipped with an energy dispersive spectrometer (EDS: EMAX, Horiba, Japan). The structure of the films was analyzed using an X-ray diffractometer (XRD: Max-2500, Rigaku B) in Cu-kα radiation with λ=1.5405 Å. Optical transmittance of the films was measured using a UV-visible spectrophotometer (V530, JASCO). The PbS thin films were assessed by X-ray photoelectron spectroscopy (XPS) using an Thermo VG XPS system (K-alpha, Thermo VG). Ultraviolet photoelectron spectroscopy (UPS: PHI 5000 Versa Probe^{TM}, ULVAC-PHI) was used to examine energy band characteristics. Current density-voltage (J-V) behavior was examined by using a current-voltage analyzer (IviumStat, Ivium Technology) and a solar simulator (Sun 2000, ABET technology) under AM 1.5. External quantum efficiency (EQE) of the cells was analyzed by an incident photon conversion efficiency measurement unit (QEX 10, PV measurements).

Results and Discussion

Fig. 1 shows the X-ray diffraction patterns of PbS films deposited on SLS substrates at 40, 60 and 80 ^{o}C. Regardless of deposition temperature, the PbS thin films were found to be well crystallized with all Bragg reflection peaks corresponding to cubic phase, which is consistent with the reference [JCPDS 05-0592]. The intensities of all the peaks tend to increase significantly with temperature, indicating that the crystallinity of the film is boosted very sensibly with the small change in temperature. The change in deposition temperature does not affect the directionality of crystal growth. The average crystalline size was calculated using

the Sherrer equation from the full width at half maximum (FWHM) of the two main (200) and (111) peaks. The crystallite size of the films deposited at 40, 60 and 80 ^{o}C was estimated to be 16, 29, and 52 nm, respectively, which suggests that the growth of crystallites is substantially enhanced by means of deposition temperature. It is understood that precursors gain a higher energy at elevated bath temperature to decompose them into sulfur and lead ions and subsequently to precipitate the nucleation and growth process of PbS.[16]

Surface SEM photographs of the PbS thin films deposited at different temperatures are shown in Fig. 2. As expected from the XRD FWHM analysis, the temperature dependence of grain size is apparent in the images. All films showed densely-packed microstructures without voids or cracks. Smaller discrete grains were distributed over the surface of the films deposited at 40 ^{o}C while more faceted larger grains were identifiable with increasing temperature up to 80 ^{o}C. In conjunction with the crystallinity evolution, the faceted grains indicate that the temperature of 80 ^{o}C is high enough to facilitate the development of well-defined grains with a rougher surface even within a short duration of 5 min.

Fig. 3 shows the plots of $(\alpha h\nu)^2$ as a function of photon energy $h\nu$, where α is the absorption coefficient, which was obtained from the spectral transmittance and reflectance curves (not shown here) for the PbS thin films processed at different temperatures. The optical band gap value was determined by extrapolating linear portions of $(\alpha h\nu)^2$ as a function of photon energy.[17] The optical band gaps of the absorbers processed at a bath temperature of 40, 60 and 80 ^{o}C were estimated to be 1.61, 1.31 and 0.92 eV, respectively. Clearly, the deposition at lower temperature leads to a larger band gap. The band gap tunability of PbS is generally understood in terms of the quantum confinement effect, which is directly related to crystallite size of quantum dots.[18] Typically, when the crystallite size of quantum dots decreases to the range of 5-18 nm, the band gap increases, which minimizes the density of localized states or defects in the forbidden band.[19] In the present case, however,

considering the size of the crystallite of the films, the quantum confinement effect may not be significant since our crystallite size is greater than 16 nm. The band gap tunability of the films having larger crystallite sizes beyond the quantum confinement regime may have different mechanism. There are numerous reports demonstrating variable band gaps of 0.9 to 2.3 eV in the case of non-colloidal PbS thin films for crystallites with the size range of 12 to 38 nm.[18-23] These studies attributed the dependence of band gap potentially due to the residual strain, defects, film thickness, grain size and morphology beyond the influence of quantum confinement effect. However, the reasons for the tunable band gaps are not clearly described. It is assumed that the larger grains observed here leave more effective unfilled inter-granular volume so that the absorption per unit thickness is reduced.[22] The larger grains at higher temperature may also induce the localized energy states from defects in grains and grain boundaries, resulting in a lowered band gap.

High resolution XPS spectra of the Pb 4f and S 2p regions for the PbS thin films deposited at different temperatures of 40, 60 and 80 ^{o}C are represented in Fig. 4. The values of the binding energy were calibrated using the C 1s peak at 285 eV as an internal standard. The XPS spectra in Fig. 4 (a) include two peaks at 137.5 and 142.5 eV, which originate from the binding energy for Pb $4f_{7/2}$, and Pb $4f_{5/2}$, respectively. The S region shown in Fig. 4 (b) consists of two peaks at 160.7 and 161.8 eV due to the S $2p_{1/2}$, and S $2p_{3/2}$ transitions, respectively. The binding energies for Pb and S are in agreement with the values reported in literature for PbS.[24,25] There is no noticeable difference in the XPS patterns obtained at the different temperature.

The variations in the atomic percentage of Pb and S on film surface according to the deposition temperature are shown in Table 1. The ratios were obtained by averaging the intensity values from the multiple-measurements of EDS. The relative percentage of S to Pb was found to decrease slightly from ~50.31 to ~50.03 % with increasing temperature from 40

to 80 ^{o}C, resulting in the decrease of the S/Pb ratio from 1.012 to 1.001. It is unclear with the reason for the ratio change sensitive to the deposition temperature. It is assumed that the result in the change of stoichiometry may be associated with the reaction sequence and kinetics in the formation process of PbS. For example, it is reported that the final decomposition of sulfur from the precursor of thiourea CH_4N_2S needs a sufficient reaction time since the formation of HS^- is involved as an intermediate step prior to the formation of PbS.[26] Since the shorter reaction time of 5 min was used at 80 ^{o}C to obtain the identical film thickness of ~200 nm (compared to 60 min at 40 ^{o}C), sulfur may be less available at the high temperature. It is also believed that the change in stoichiometry at each temperature affects the growth degree of crystals during the deposition. A relatively higher content of Pb at high temperatures may act positively in facilitating crystal growth of PbS.

Table 1 also represents carrier concentration according to the deposition temperature, which was measured by the Hall measurement. All samples showed p-type conductivity. Increasing the deposition temperature from 40 to 80 ^{o}C resulted in the decrease of the carrier concentration from 5.59 x 10^{16} to 8.93 x 10^{14} cm^{-3}. Kim et al. reported that a small change of 0.08% in the S/Pb ratio in PbS would bring the energy difference between the valence band edge and the Fermi level by as much as 0.15 eV.[27] Aside from the potential effect of the S/Pb ratio on carrier concentration, the surface roughness and nature of grain boundary may affect largely the mobility of carriers at each temperature. Roughened interfaces and the discontinuity at grain boundaries impede favorable transfer of charges. It is conclusive that the deposition temperature in CBD determines not only the microstructural features like crystallite size and roughness but also the stoichiometry of film surface, which potentially influences the photovoltaic performance.

UPS spectra for the PbS thin films with different band gaps were examined to determine the band alignment with respect to the CdS films. Fig. 5(a) and (b) show the UPS spectra of

the PbS thin films processed at different temperatures. Valence band energy with respect to the Fermi energy level was determined by extrapolating the linear portion of the low binding energy side as illustrated in Fig. 5(a). Work function of the PbS thin films was determined by the intersection of the secondary electron cut-off that occurs at high binding energies (Fig. 5(b)). The measured work functions of the PbS thin films were -4.43, -4.41, and -4.34 eV for band gaps of 0.92, 1.31, and 1.61 eV, respectively. The valence and conduction band edges of the PbS films were calculated from the work function and optical band gap values.

Fig. 6 shows the schematic energy band diagrams of the PbS thin films with different band gaps, which were obtained by the UPS analysis. The band diagram of the CdS film was also included for elucidating ideal band alignments with PbS. The separate UPS spectrum was analyzed for the CdS layer (not shown here). The relative position of all energy levels, i.e., conduction band edge, valence band edge and Fermi energy level, with respect to the vacuum level, tended to decrease slightly toward the lower band gap of PbS from 1.61 to 0.92 eV. The valence band edge of the CdS layer is far below that of the PbS thin films since CdS has a wide band gap of 2.61 eV. Such wide band gap is expected to result in a large hole injection barrier at the PbS/CdS interface, which enhances the device performance instead of decreasing the efficiency.[28,29] Furthermore, the electron back transfer from the CdS to the PbS absorber must be suppressed for more efficient heterojunction solar cells.[30] It can be achieved by increasing the conduction band offset between the CdS and PbS layers. Thus, a larger conduction band offset ΔE_c lowers the loss of the photogenerated carriers resulting in a higher conversion efficiency.[13,30] From the analysis of the UPS results here, ΔE_c was estimated to be about 0.96, 0.63, and 0.27 eV for the PbS films with band gap of 1.61, 1.31, and 0.92 eV, respectively. Therefore, the photoexcited electron injection into the CdS layer will be the most energetically favorable for the 1.61 eV PbS film owing to the larger conduction band offset.

Fig. 7 shows the current density-voltage curves of the PbS/CdS cells incorporating different band gap of PbS. The resulting photovoltaic values of short circuit current density J_{sc}, open circuit voltage V_{oc}, fill factor FF and conversion efficiency η are presented in Table 2. As expected, the photovoltaic characteristics seem to be directly related to the band gap of the PbS absorber. The photovoltaic cells with PbS processed at 40 ^{o}C (or having a large band gap of 1.61 eV) had the best efficiency of ~3.10% with J_{sc} of 20.93 mA/cm^2, V_{oc} of 280 mV and FF of 52.70%. The cells with the lower band gap of PbS processed at higher temperatures exhibited inferior photovoltaic performances. V_{oc} is known to be particularly related to the band gap of the absorber as illustrated by the simple equation, $V_{oc} = A(E_g/e) - B$, where e is the electron charge, E_g is the band gap of the absorber layer, and A and B are the constants.[31] Accordingly, a larger band gap results in a higher V_{oc} value. On the other hand, the J_{sc} and FF values are likely affected by the light absorption and effective hole carrier density of the absorber. The light absorption is strongly dependent on the band gap of absorbers. As an ideal case of solar cells, band gap of ~1.3 - 1.5 eV is favorable to obtain an appropriate amount of photoexcited electrons because the wavelengths corresponding to these energies show the highest intensity of solar spectrum on the surface of earth. In our case, the PbS layer with E_g ~ 1.61 eV that is close to the ideal band gap range demonstrates a larger conduction band offset with CdS and thus a higher driving force for carrier transfer. Similarly, Bhandari et al. reported that the PbS quantum dot absorbers with a band gap of ~1.57 eV gave rise to an efficient solar cell due to promising conduction band offset and effective light absorption.[13]

Fig. 8 shows normalized EQE spectra of the PbS/CdS solar cells for the PbS thin films with different band gaps. The falling edge of the spectra gradually shifts towards higher wavelength consistent with the decreasing band gap of the PbS films. For the 1.61 eV film, the photocurrent generated in the region 470 to 750 nm is attributed to the absorption in the PbS films followed by electron transfer to the CdS layer. The curve below ~470 nm

represents photocurrent contributed by the CdS film which absorbs the wavelength above the band gap of 2.61 eV. As the band gap of the PbS film decreases, the absorption range increases with the extended tail. The higher absolute EQE values of solar cells for the PbS film with the band gap of 1.61 eV imply more efficient charge separation, transportation and collection as generally accepted for the enhanced EQE values. Absolute EQE spectra of the photovoltaic cells for the PbS thin films processed at different temperatures are presented in Fig. S1. Calculated J_{sc} values by integration of the curves are 19.48, 9.07 and 2.56 mA/cm^2 for the PbS films with band gap of 1.61, 1.31, and 0.92 eV, respectively. They are in good agreement with the J_{sc} values in Table 2.

Conclusions

The positive adjustment of processing parameter in chemical bath deposition of PbS has shown the enhanced photovoltaic cell efficiency of ~3.1 % for PbS/CdS thin film solar cells, which is the best efficiency so far without the involvement of quantum dots. As the critical origin of the enhancement, proper band alignment between PbS and CdS layers is believed to influence efficiently the light absorption and charge transfer only for the PbS case having the highest optical band gap of ~1.61 eV. The achievement is possible by reducing deposition temperature to near room temperature of 40 ^{o}C to minimize the crystalline size of PbS as small as 16 nm, which result in the largest conduction band offset of 0.96 eV. In conjunction with the level of crystalline size, smoother S-rich surface is assumed to contribute to the improved carrier concentration and photovoltaic properties for the case of the band gap of 1.61 eV. Other photovoltaic values of J_{sc} of 20.93 mA/cm^2, V_{oc} of 280 mV and FF of 52.70% are obtained for the PbS absorber exhibiting the best conversion efficiency.

Acknowledgements

This work was financially supported by a grant of the National Research Foundation of Korea (2011-0020285).

References

1 L. Yu, Y. Lv, G. Chen, X. Zhang, Y. Zeng, H. Huang and Y. Feng, *Inorg. Chim. Acta.*, 2011, 376, 659-663.

2 S. M. Lee and Y. S. Cho, *J. Alloys Compd.*, 2013, 579, 279-283.

3 W. Ji, P. Jing, W. Xu, X. Yuan and Y. Want, *Appl. Phys. Lett.*, 2013, 103, 053106.

4 G. I. Koleilat, L. Levina, H. Shukla, S. H. Myrskog, S. Hinds, A. G. Pattantyus-Abraham and E. H. Sargent, *ACS Nano*, 2008, 5, 833-840.

5 W. Lee, S. K. Min, V. Dhas, S. B. Ogale and S. H. Han, *Electrochem. Commun.*, 2009, 11, 103-106.

6 A. S. Obaid, Z. Hassan, M. A. Mahdi and M. Bououdina, *Sol. Energy*, 2013, 89, 143-151.

7 H. Noguch, A. Setiyadi, H. Tanamura, T. Nagatomo and O. Omoto, *Sol. Energ. Mat. Sol. C.*, 1994, 35, 325-331.

8 K. T. R. Reddy, N. K. Reddy and R. W. Miles, *Sol. Energ. Mat. Sol. C.*, 2006, 90, 3041-3046.

9 P. Sinsermsuksakul, J. Heo, W. Noh, A. S. Hock and R. G. Gordon, *Adv. Energy Mater.*, 2011, 1, 1116-1125.

10 J. M. Luther, J. Gao, M. T. Lloyd, O. E. Semonin, M. C. Beard and A. J. Nozik, *Adv. Mater.*, 2010, 22, 3704-3707.

11 T. Ju, R. L. Graham, G. Zhai, Y. W. Rodriguez, A. J. Breeze, L. Yang, G. B. Alers and S. A. Carter, *Appl. Phys. Lett.*, 2010**,** 97, 043106.

12 H. Moreno-Garcia, M. T. S. Nair and P. K. Nair, *Thin Solid Films*, 2011, 519, 2287-2295.

13 K. P. Bhandari, P. J. Roland, H. Mahabaduge, N. O. Haugen, C. R. Grice, S. Jeong, T.

Dykstra, J. Gao and R. J. Ellingson, *Sol. Energ. Mat. Sol. C.*, 2013, 117, 476-482.

14 J. Hernandez-Borja, Y. V. Vorobiev and R. Ramirez-Bon, *Sol. Energ. Mat. Sol. C.*, 2011, 95, 1882-1888.

15 A. K. Rath, M. Bernechea, L. Martinez and G. Konstantatos, *Adv. Mater.*, 2011, 23, 3712-3717.

16 A. Osherov, V. Ezersky and Y. Golan, *J. Cryst. Growth*, 2007, 308, 334-339.

17 B. C. Mohanty, D. H. Yeon, B. K. Kim and Y. S. Cho, *J. Electrochem. Soc.*, 2011, 158, P30-P35.

18 S. B. Pawar, J. S. Shaikh, R. S. Devan, Y. R. Mac, D. Haranath, P. N. Bhosale and P. S. Patil, *Appl. Surf. Sci.*, 2011, 258, 1869-1875.

19 M. M. Abbas, A. Ab-M. Shehab, N-A. Hassan, A-K and Al-Samuraee, *Thin Solid Films*, 2011, 519, 4917-4922.

20 K. C. Preetha and T. L. Remadevi, *Mat. Sci. Semicon. Proc.*, 2013, 16, 605-11.

21 R. K. Joshi, A. Kanjilal and H. K. Sehgal. *Appl. Surf. Sci*., 2004, 221, 43-47.

22 P. Prathap, N. Revathi, Y. P. V. Subbaiah and K.T. R. Reddy, *J. Phys: Cond. Matt*., 2008, **20**, 035205.

23 S. Jana, S. Goswami, S. Nandy and K. K. Chattopadhyay, *J. Alloy. Compd*., 2008, **481**, 806-810.

24 J. D. Patel, F. Mighri, A. Ajji and T. K. Chaudhuri, *Mater. Chem. Phys.*, 2012, **132**, 747-755.

25 S. Chen and W. Liu, *Mater. Chem. Phys.*, 2006, **98**, 183-189.

26 R. Ortega-Borges and D. Lincot, *J. Electrochem. Soc.*, 1993, **140**, 3464-3473.

27 D. Kim, D. Kim, J. Lee and J. C. Grossman *Phys. Rev. Lett.*, 2013, **110**, 196802.

28 P. K. Nair, E. Barrios-Salgado, J. Capistrain, M. L. Ramon, M. T. S. Nair and R. A. Zingaro, *J. Electrochem. Soc*., 2010, **157**, D528-D537.

29 X. Wang, G. I. Koleilat, J. Tang, H. Liu, I. J. Kramer, R. Debnath, L. Brzozowski, D. A. R. Barkhouse, L. Levina, S. Hoogland and E. H. Sargent, *Nat. Photonics*, 2011, **5**, 480-484.

30 A. G. Pattantyus-Abraham, I. J. Kramer, A. R. Barkhouse, X. Wang, G. Konstantatos, R. Debnath, L. Levina, I. Raabe, M. K. Nazeeruddin, M. Gratzel and E. H. Sargent, *ACS Nano,* 2010, **4**, 3374-3380.

31 C. Y. Kuo, M. S. Su, Y. C. Hsu, H. N. Lin and K. H. Wei. *Adv. Funct. Mater.*, *2*010, **20**, 3555-3560.

Table 1 Atomic percentage, S/Pb ratio and carrier concentration of PbS thin films deposited at different temperatures of 40, 60 and 80 ^{o}C. The relative atomic percentages were obtained by the EDS analysis of film surface.

T (^{o}C)	Atomic percentage (%)		S/Pb	Carrier concentration (cm^{-3})
	Pb	S		
40	49.69	50.31	1.012	5.59×10^{16}
60	49.87	50.13	1.005	1.36×10^{15}
80	49.97	50.03	1.001	8.93×10^{14}

Table 2 Optical band gap of PbS thin films and photovoltaic parameters of PbS/CdS solar cells under 100 mW/cm^2 illumination

T (^{o}C)	E_g (eV)	J_{sc} (mA/cm^2)	V_{oc} (mV)	FF (%)	η (%)
40	1.61	20.93	280	52.70	3.10
60	1.31	11.12	214	40.36	0.96
80	0.92	3.30	180	29.13	0.19

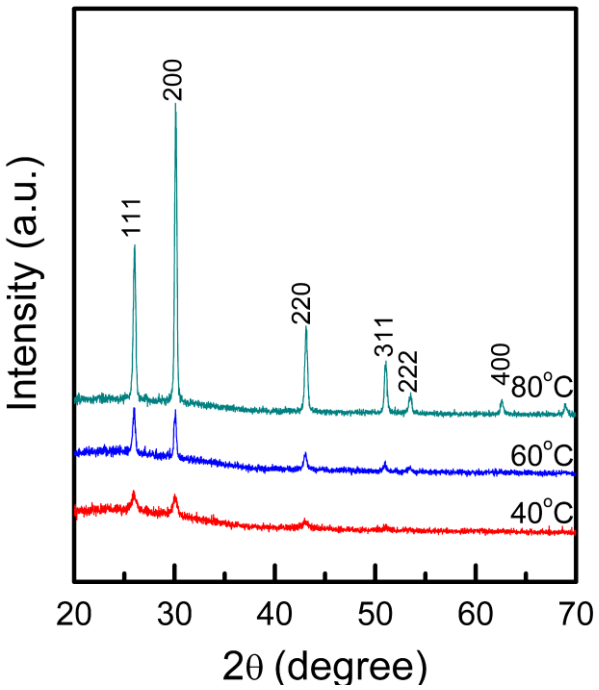

Fig. 1 XRD patterns of PbS thin films deposited on SLS glass substrate at different temperatures of 40, 60 and 80 ^{o}C by chemical bath deposition.

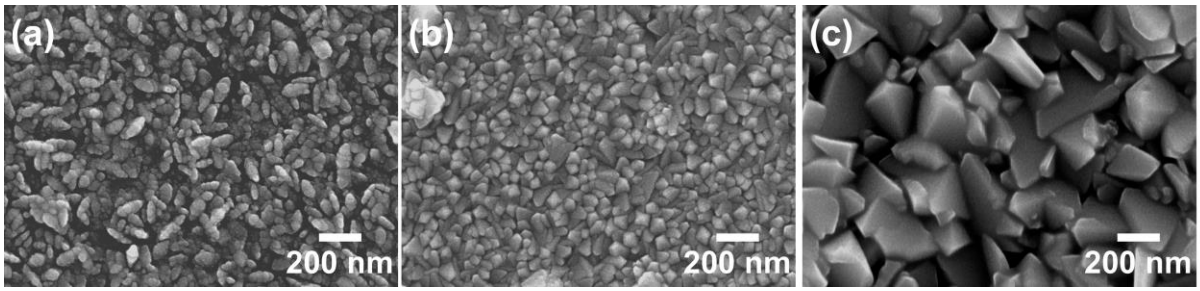

Fig. 2 SEM surface images of PbS thin films deposited at different temperature of 40, 60 and 80 ^{o}C for 60, 30 and 5 min, respectively.

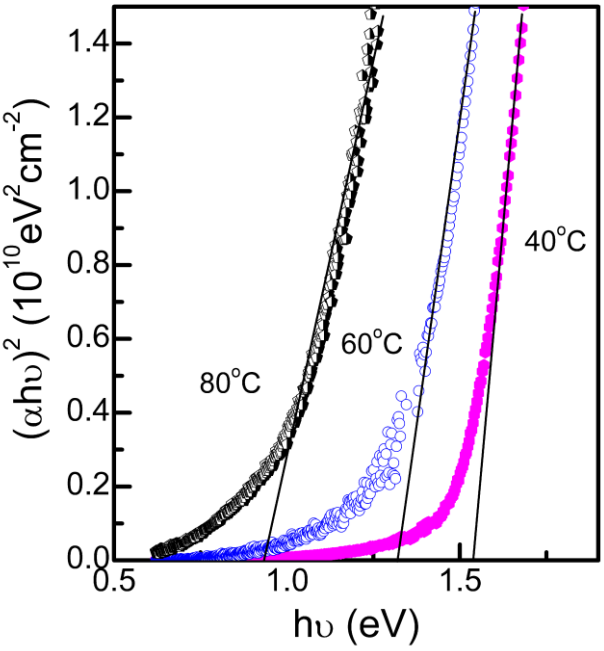

Fig. 3 $(\alpha h\nu)^2$ vs. $h\nu$ plots for PbS thin films deposited at different temperatures of 40, 60, and 80 ^{o}C. Optical band gap of the film is determined by extrapolating the curve from the upper linear region to $(\alpha h\nu)^2 = 0$ as illustrated by the straight line of each curve.

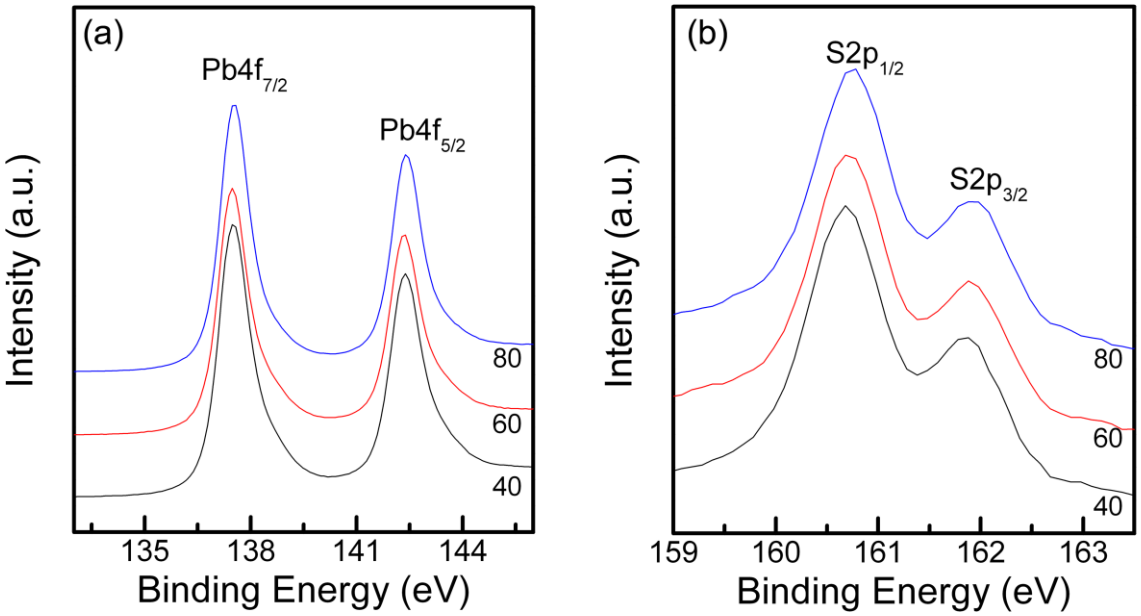

Fig. 4 XPS spectra of PbS thin films deposited at 40, 60 and 80 ^{o}C in the binding energy regions corresponding to (a) Pb 4f and (b) S 2p peaks.

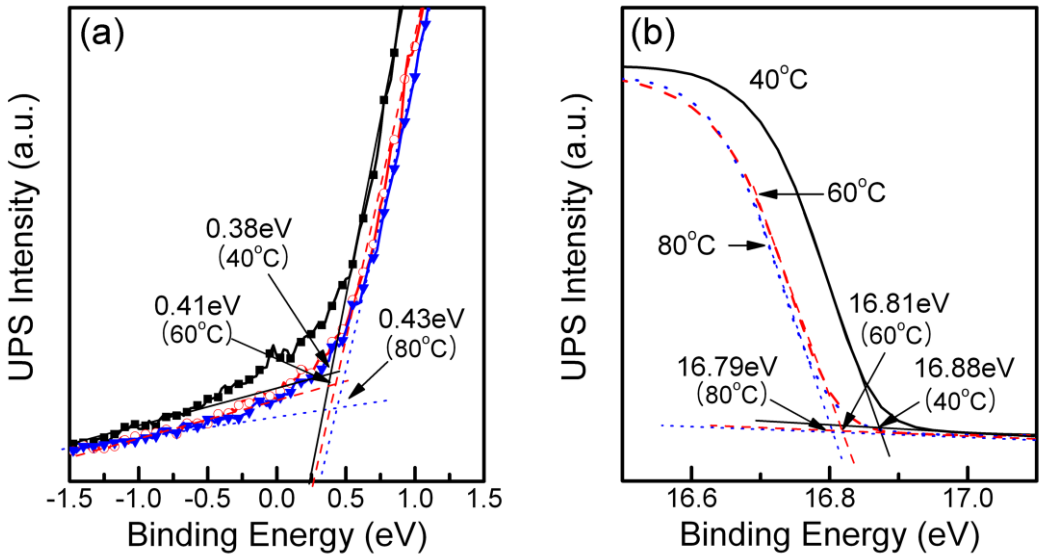

Fig. 5 UPS cutoff spectra in the two binding energy regions of (a) -1.5 to +1.5 eV and (b) 16.4 to 17.2 eV for the PbS thin films deposited at 40, 60, and 80 °C.

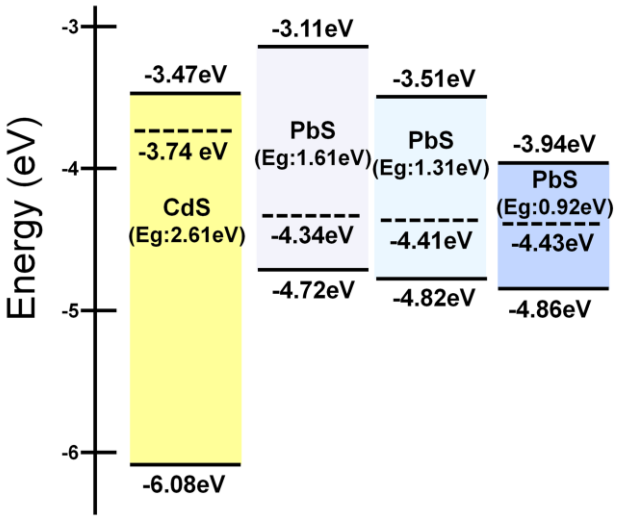

Fig. 6 Schematic of the energy level alignments at the junction of the PbS and CdS layers for the different optical band gaps of PbS, obtained by the UPS analysis of Fig. 5. The dotted line indicates the Fermi energy level.

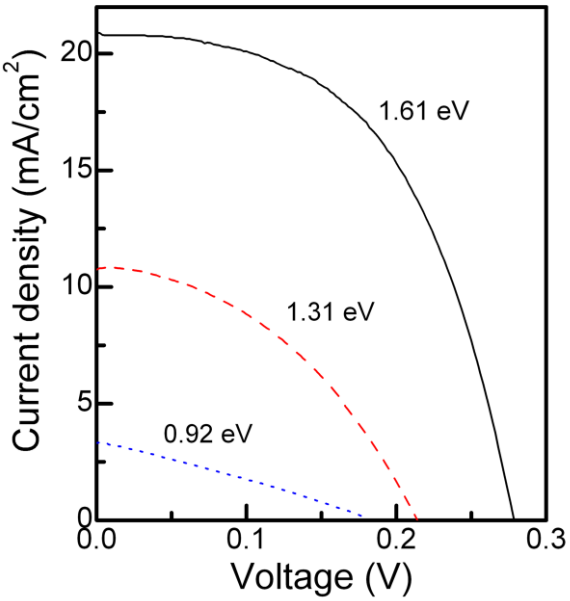

Fig. 7 Current density vs. voltage plots for the photovoltaic cells with different band gaps of the PbS thin film.

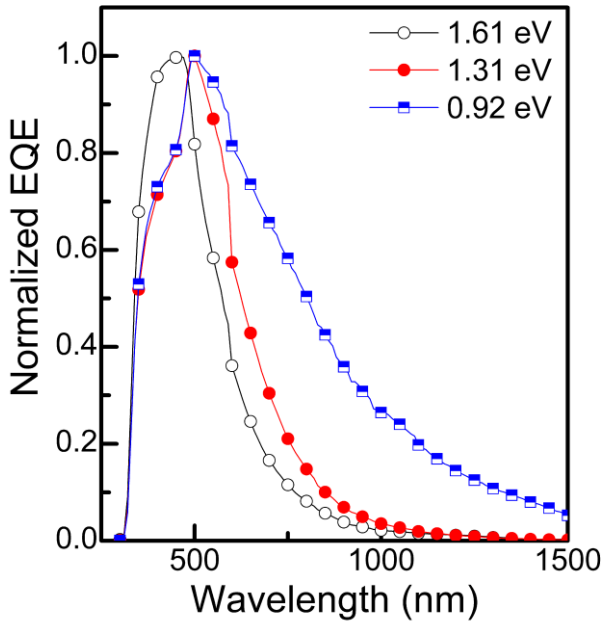

Fig. 8 Normalized EQE spectra of the photovoltaic cells for the PbS thin films with different band gaps.